RANS-VOF modelling of the hydraulic performance of the LOWREB caisson

I. López[a,c], P. Rosa-Santos[b,c], C. Moreira[c], F. Taveira-Pinto[b,c]

[a] *Universidade de Santiago de Compostela, Hydraulic Engineering, Campus Universitario s/n, 27002, Lugo, Spain*

[b] *CIIMAR, Interdisciplinary Centre of Marine And Environmental Research of the University of Porto, Terminal de Cruzeiros do Porto de Leixões, Avenida General Norton de Matos, S/N, 4450-208 Matosinhos, Portugal*

[c] *FEUP - Faculty of Engineering of the University of Porto, Department of Civil Engineering, rua Dr. Roberto Frias, s/n, 4200-465, Porto, Portugal*

Abstract

The LOWREB caisson is an innovative multi-chambered, low-reflection structure that incorporates inner weirs at each dissipative chamber to promote wave energy dissipation. It was designed to be applied either as external caisson breakwater or as low reflection quay-wall. In this paper, the OpenFOAM® CFD numerical package was used to implement a RANS-VOF numerical model of the LOWREB caisson concept, which was then validated using results from experimental tests in a two-step approach: qualitatively, by comparing the "wave-structure" interaction on both physical and numerical models, and quantitatively, by comparing the reflection coefficients determined from the results of the numerical model simulations and those from the physical model tests. Once validated, the numerical model was used to carry out a comprehensive study of the hydrodynamic behavior of the LOWREB caisson aiming the understanding of the wave energy dissipation mechanisms and the assessment of its hydraulic efficiency with respect to wave reflection under an extended range of hydrodynamic conditions (*e.g.*, water levels, wave heights, and wave periods). The numerical study confirmed the importance of the inner weirs on the wave energy dissipation. The hydraulic efficiency of the LOWREB caisson was found to be highly influenced by the combined effect of the wave period and water level. However, the influence of the wave height is not negligible: in general, energy dissipation increases with the wave height. Overall, the LOWREB caisson presents its best performance for the high and mean water level conditions, with all the values of the reflection coefficient below 70% and most of them in the range 30%-60%. The worse results obtained for the lower water level were attributed to the difficulties that waves have to overtop the weirs and enter the dissipative chambers, for this water level. In addition, streamlines, velocity and vorticity fields enabled obtaining important insights on the wave energy dissipation processes that take place during the wave-structure interaction, which results in the development of several vortices, not only inside the dissipative chambers, but also in front of the structure.

Keywords

wave reflection; low-reflection structure; wave-structure interaction; LOWREB; numerical modelling; OpenFOAM

1. Introduction

Sea ports should provide shelter and quiet conditions for the safe berthing and mooring of ships, as well as to enable an efficient handling of cargos. In a first instance, those conditions are ensured by breakwaters, which prevent sea wave propagation into the inner harbour basins and may also promote the dissipation of its energy (Rosa-Santos and Taveira-Pinto, 2013). Inside the harbour basin, additional wave energy dissipation may occur if low reflective solutions are chosen for the port terminals and other internal boundaries (Taveira-Pinto *et al*., 2011). Soft countermeasures, such as tension mooring (Rosa-Santos *et al*., 2014), may also be used to reduce downtime and avoid mooring problems at ocean facing ports, which are often related with excessive motions of

the moored ships caused directly by wave action or indirectly by wave related phenomena (López and Iglesias, 2014; López *et al.,* 2015), namely wave reflection.

Rubble-mound structures have good wave dissipation characteristics, but sometimes are an infeasible option due to economical or technical constrains. In this case, perforated-wall caisson breakwaters may be used to avoid the drawbacks of the traditional vertical breakwaters (Suh *et al*., 2006), which have a high reflective behaviour, ensuring better ship navigation and manoeuvring conditions in its vicinity and also lower wave disturbance in the internal harbour basins.

Jarlan (1961) proposed the first concept of a perforated caisson breakwater: it consists of a perforated front wall, a solid back wall and one wave-dissipating chamber between them. After that pioneering work, modifications to the so-called Jarlan type breakwater have been proposed and studied, for instance including two (Li *et al*., 2003) or multiple (Huang, 2006) wave-dissipating chambers, internal horizontal perforated plates (Yip and Chwang, 2000; Hu *et al*., 2002), slightly inclined porous plates (Cho and Kim, 2008), as well as internal wave-dissipating chambers partially or completely filled with rocks of one (Isaacson *et al*., 2000) or two different gradings (Liu *et al*., 2007). Less conventional alternatives were also studied, as the concentric two-cylinder structures composed of an internal impermeable cylinder and an external thin and porous wall (Song and Tao, 2007). These solutions reduce both the transmitted and the reflected wave energy as well as the hydrodynamic loading on the structure. In fact, the incident wave energy is partly reflected at the perforated seaward wall and partly transmitted through the openings to the wave-dissipating chambers, in which energy dissipation occurs due to resonance phenomena, vortices and friction losses. Those physical processes are governed mainly by the porosity of the perforated wall and by the wave chamber width.

In order to reduce the wave disturbance within the port, several dissipative (or anti-reflective) concrete blocks were also developed for berthing structures and harbour basin slopes: Igloo blocks (Bottin, 1976), WAROK blocks (Ijima *et al.*, 1976), BARRA blocks (Berenguer and Arana, 2002), NOREF blocks (Taveira-Pinto *et al*., 2011), among others. As their counterparts designed for applications in breakwaters, the structures built with those blocks absorb a fraction of the incident wave energy by turbulence, viscous friction and resonance. In addition, non-conventional and traditional designs of wave absorbing quay-walls, consisting of a single partial wave chamber, with limited height and depth above and below the water level, filled with natural stones placed to form a rubble mound with a certain slope and porosity, were also proposed and studied (Theocharis *et al*., 2011; Altomare and Gironella, 2014). Huang *et al*. (2011) presents a comprehensive review on the hydraulic performance and wave loadings of perforated and slotted coastal structures.

Many of the low reflection concepts initially developed for breakwaters can also be adapted and applied in port terminals (*e.g.* Liu and Faraci, 2014). The adaptations are essentially motivated by the different functions of the structures, local water depths and wave conditions. In fact, the external breakwaters are exposed to unhindered extreme waves, whereas nearby the port terminals smaller waves are expected, since only a fraction of the wave energy can enter the port and the waves generated locally by wind and passing ships are small both in terms of height and period.

Pinto (2012) proposed a new concept of a low reflection structure, the LOWREB caisson, which is suitable for both applications, external caisson breakwaters and inner low reflective quay-walls, that is composed of one or more dissipative wave chambers, with varying bottom elevations and widths, separated by perforated-walls with pre-defined porosities. The main innovation in the LOWREB caisson are the inner weirs located at each dissipative chamber. The experimental proof of concept of this novel caisson showed that it is a valid concept for

marine applications, namely harbour breakwaters and quay-walls, because of its wave energy dissipation capacity, for which the inner weirs were found to play a major role (Ciocan *et al.,* 2017).

Physical modelling is a valuable and reliable tool to evaluate the effectiveness of low reflection structures, being widely applied in the proof of concept testing of new concepts (*e.g*., Taveira-Pinto *et al*., 2011; Theocharis *et al*., 2011). However, since experimental studies are often expensive and time-consuming, the characterization of the reflection characteristics of the structures is carried out only for a limited number of wave conditions and setups. Therefore, the simulation of the interactions between the incident waves and the low reflection structures is also important for a detailed characterization of their hydraulic efficiency with regard to wave reflection, and a more comprehensive understanding of the wave energy dissipation mechanisms.

In this respect, different mathematical and numerical approaches have been developed and successfully validated with experimental data, namely: analytical and semi-analytical methods based on potential flow theory (*e.g*., Liu *et al*., 2007; Liu *et al.,* 2008), semi-empirical methods based on multi-parametric nonlinear regression tools (*e.g*., Garrido and Medina, 2012), computational fluid dynamic (CFD) models (Lee *et al*., 2017), among others. However, since viscous effects of boundary layer separation, turbulence, wave breaking and overtopping are important in this kind of applications (Fugazza and Natale, 1992; Ciocan *et al.*, 2017), CFD models based on the Navier Stokes equations are, in principle, more appropriate for the simulation of wave-structure interactions, by accounting the most relevant physical phenomena affecting the dissipation of wave energy.

The application of the Reynolds–Averaged Navier Stokes (RANS) equations to model wave-structure interactions has evolved significantly in the last decades, being now possible to study perforated and permeable structures at reasonable level of detail and accuracy, with only a few simplifications in the translation of the problem physics. In fact, the range of application of such models is very wide, extending from the traditional coastal engineering problems (Higuera *et al*., 2013) to the development and optimization of marine renewable energy technologies (Lopez *et al*., 2014). In addition, RANS models have already been successfully validated for the simulation of several complex hydrodynamic phenomena in the coastal and port engineering fields. Their principal drawback is the high computational power required.

Presently, RANS models are able to realistically generate ocean waves and also integrate active wave absorption methods (*e.g*., del Jesus *et al*., 2012; Higuera *et al*., 2015; Vanneste and Troch, 2015). Physical phenomena such as wave breaking, run up, run down, bottom friction, wave interaction with porous structures, wave overtopping, and wave energy dissipation are also reproduced with a satisfactory level of detail and accuracy (*e.g*., Lara *et al*., 2012; Higuera *et al*. 2014a; Jensen *et al*., 2014; Wu *et al*., 2014), making possible their application in practical coastal engineering problems (*e.g*., Higuera *et al*., 2014b). One of the greatest advantages of the CFD models is their intrinsic ability of providing pressure and velocity profiles in different locations of the structure, allowing a more comprehensive understanding of the problem physics, still with a high level of fidelity and still relatively time-efficient when compared to physical model testing.

In this paper, the CFD code OpenFOAM® is used to study the interaction of waves with the LOWREB caisson, in order to better characterize its hydrodynamic response with regard to wave reflection for a wide range of test conditions, covering typical applications of this novel caisson in breakwaters and quay-walls. The results of the experimental proof of concept tests (Ciocan *et al.,* 2017) are used in the validation of the numerical model. The numerical simulations are also explored to gain a more comprehensive insight into the wave energy dissipation mechanisms of this caisson concept, looking at its future optimization.

This paper is structured as follows. The LOWREB caisson concept is briefly described in Section 2, together with the main conclusions of the previous experimental proof of concept tests. The numerical approach applied and the testing programme is presented in Section 3. Then, Section 4 describes the validation of the numerical model as well as the novel insights on the hydrodynamic performance of the LOWREB caisson. The validated numerical model is applied to characterize the performance of the structure for the new hydrodynamic conditions and the results are discussed. Finally, the summary and conclusions are given in Section 5.

2. The LOWREB caisson

The LOWREB caisson is composed of one or more dissipative chambers with varying bottom elevations (and widths), separated by perforated-walls with pre-defined porosities, similarly to other low reflection structures. The main innovation in this concept is the inner weirs, located at the beginning of each dissipative chamber, Figure 1, which introduce additional dissipation mechanisms. The shape of the weirs was designed to favour water movement in the rear wall direction, reducing wave reflection. The return flow over the weirs falls in the water nappe created by the lower weir and so on, creating a succession of free falling nappes at each weir edge. This process generates intense turbulence, flow aeration and, therefore, energy dissipation (Ciocan *et al*., 2016).

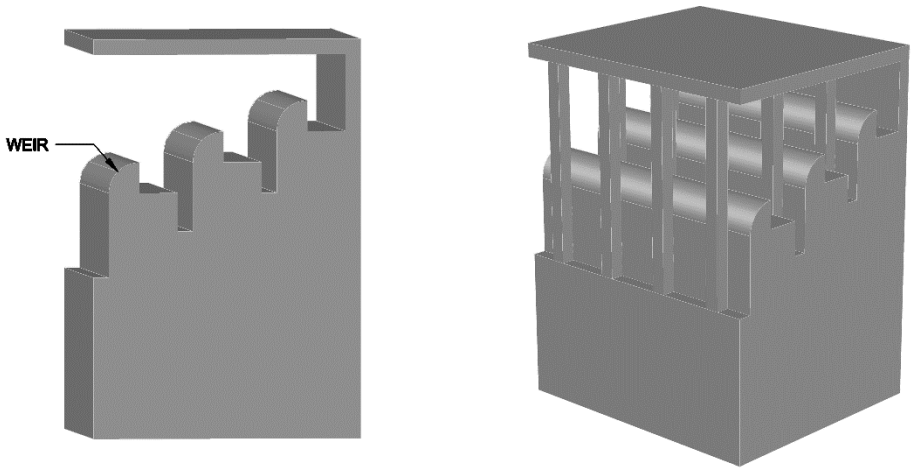

Figure 1 – LOWREB caisson: 3D perspectives.

The height of the successive LOWREB chambers reduces in the rearward direction to materialize the "cascade" of weirs and to improve the overall stability of the structure, due to the extra weight added to the lower part of the caisson. The space behind each weir (i.e., below its crest level, Figure 1) can be filled with rubble to improve energy dissipation and to increase the stability of the caisson. The LOWREB concept was developed to be used in external caisson breakwaters or inner low reflective quay-walls (Ciocan *et al*., 2016).

Owing to the complexity of the LOWREB geometry and the hydraulic processes associated to the wave-structure interaction, there are no general design criteria to be followed. Hence, the preliminary design of this caisson was based on existing knowledge about low reflection, perforated structures (*e.g*., Williams et al., 2000; Bergmann and Oumeraci, 2001; Chen et al., 2002; Li et al., 2003; Huang, 2006). For example, for increased energy dissipation, a perforated and multi-chambered caisson was proposed, with the porosities of the perforated-walls decreasing gradually along the incident wave direction.

A LOWREB caisson consisting on a three-chamber, perforated-wall structure with inner weirs was tested in the wave basin of the Hydraulics Laboratory of the Hydraulics, Water Resources and Environment Division of the Faculty of Engineering of the University of Porto, Portugal. This proof of concept study aimed at confirming the initial design of the LOWREB caisson, by assessing the impact of the inner weirs on wave energy dissipation and by evaluating the efficiency of this new caisson in the reduction of the reflected wave energy. Hence, three physical models with the same overall geometry and dimensions but different wall porosities and vertical slots' arrangements were built on a geometrical scale of 1:50 and tested under the same hydrodynamic conditions to study how these affect the LOWREB performance. The experimental tests covered only two water levels and a limited number of wave conditions.

The experimental study confirmed that the LOWREB caisson is a valid concept for harbour structures, due to its wave energy dissipation capacity, for which the inner weirs were found to play a major role. In fact, the variation of the reflection coefficient between the three tested models with varying porosity was negligible being this result attributed to the very large porosities considered in the study (67 and 80%). The obtained results suggest that the perforated structures considered were transparent to the incident waves and that the wave energy dissipation was, essentially, governed by the inner weirs, which induce vortexes, air entrainment and intense turbulence, therefore confirming the innovative character of the LOWREB caisson (Ciocan *et al.*, 2016).

The experimental results also indicate that the hydraulic efficiency of the LOWREB caisson increases with the wave height for the lower water level and with the wave period for the highest. Greater efficiency with respect to wave reflection was accomplished for the highest water level. For the lower water level, the LOWREB caisson roughly performed as an impervious structure for the waves with the smaller heights.

Since the importance of the inner weirs was clearly demonstrated experimentally, it is now of interest to obtain more insight about the wave energy dissipation processes directly related to those elements (*i.e.*, the innovative part of the LOWREB caisson), and to assess the LOWREB hydraulic efficiency with respect to wave reflection for an extended range of hydrodynamic conditions, including applications, not only as external breakwater, but also as a low-reflection inner quay-wall.

3. Materials and methods

3.1. Numerical model

As aforementioned, the numerical study of the LOWREB caisson was carried out by means of the open-source CFD package OpenFOAM® v4.1, a set of C++ libraries to solve complex problems, among them fluid flows and turbulence, using finite volume discretization (OpenFOAM®). Moreover, the OpenFOAM® package includes mesh generation tools and pre- and post-processing utilities.

The calculations were performed by using the *interFoam* solver, which solves the Reynolds Averaged Navier–Stokes (RANS) equations for two incompressible phases. The RANS equations describe the motion of a fluid by the mass conservation (Eq.1) and momentum conservation (Eq.2) equations:

$$\nabla \cdot \mathbf{U} = 0 \ , \tag{1}$$

$$\frac{\partial \rho \mathbf{U}}{\partial t} + \nabla \cdot \left(\rho \mathbf{U}\mathbf{U} \right) - \nabla \cdot \left(\mu_{eff} \nabla \mathbf{U} \right) = -\nabla p^{*} - \mathbf{g} \cdot \mathbf{x} \nabla \rho + \nabla \mathbf{U} \cdot \nabla \mu_{eff} \ , \tag{2}$$

where $\mathbf{U}$ is the fluid velocity vector, ρ is the fluid density, p^* is the pseudo-dynamic pressure, $\mathbf{g}$ is the acceleration of gravity, $\mathbf{x}$ is the position vector, and μ_{eff} is the effective dynamic viscosity, which considers the

molecular dynamic viscosity plus the turbulent viscosity given by the turbulence model. In this study, the turbulence model selected was the renormalization group (RNG) k–ε model (Yakhot *et al.*, 1992). The RNG k–ε model attempts to address some of the weaknesses of the standard k–ε model by accounting for the contribution of smaller scales of motion, and it was already used successfully for solving similar coastal engineering problems (*e.g.*, Lin *et al.*, 2017).

The volume of fluid (VOF) method (Hirt and Nichols, 1981) was used for tracking of the water free surface. In this method, a phase function (α) indicates the quantity of water per unit volume at each cell. Therefore, when a cell is full of water, the value of the volume fraction function is $\alpha = 1$; when the cell is empty of water (full of air), it is $\alpha = 0$; and when the interface cuts the cell, the function takes a value between 0 and 1. In OpenFOAM® the volume fraction is solved by an advection equation:

$$\frac{\partial \alpha}{\partial t} + \nabla \cdot \left(\mathbf{U} \alpha \right) + \nabla \cdot \left[\mathbf{U}_c \alpha \left(1 - \alpha \right) \right] = 0 \ , \tag{3}$$

where $\mathbf{U}_c$ is the artificial compressive velocity which contributes to limit the smearing of the interface.

The pressure–velocity coupling is solved using the PIMPLE algorithm: a combination of PISO (pressure implicit with splitting of operators) and SIMPLE (semi-implicit method for pressure-linked equations) algorithms. A detailed explanation of these algorithms can be found in Jasak (1996).

For wave generation and absorption, the *waves2Foam* open-source toolbox (Jacobsen *et al*., 2012) was used. This toolbox allows the generation of regular waves of different theories including, among others, Stokes first, second and fifth order, as well as irregular waves. Regarding the absorption of reflected waves, *waves2Foam* incorporates the relaxation zone technique. In this method, the fluid velocity and the volume fraction are relaxed at every time step towards target values, following:

$$\phi = \alpha_R \phi_{\text{computed}} + \left(1 - \alpha_R \right) \phi_{\text{target}} \tag{4}$$

where ϕ can be either $\mathbf{U}$ or α, and α_R is the relaxation function formulated as follows:

$$\alpha_R \left(\chi_R \right) = 1 - \frac{\exp\left(\chi_R^{3.5} \right) - 1}{\exp\left(1 \right) - 1} \quad \text{for } \chi_R \in \left[0,1 \right] \ , \tag{5}$$

being χ_R the length scale along the relaxation zone. Thus, the relaxation function decreases from 1 at the beginning of the relaxation zone, to 0 at the end of this zone. In order to prevent any wave reflection, the relaxation zone should be sufficiently long.

For all the simulations ran, the time step was automatically controlled and adjusted at each iteration by the Courant number (C) in such a way that $C \leq 0.25$, ensuring numerical stability. This methodology led to time steps around 10^{-4} s.

3.2. Computational domain and boundary conditions

The computational domain is a reproduction of the experimental set-up (Ciocan *et al*., 2017): a wave flume with a small-scale LOWREB model (1:50) located at the end (Figure 2). Two main differences should be pointed out. First, the width of the numerical wave flume was reduced to one cell. Second, its effective length was reduced compared with that of the experimental configuration, intending to diminish the computational cost of the tests. In any case, the length of the numerical flume allows, for all the wave conditions tested, the development of, at least, two wave lengths between the generation zone and the LOWREB model. Figure 2 also shows the location

of the wave gauges (WG) and the extreme water levels studied: High Water Level (HWL) and Low Water Level (LWL).

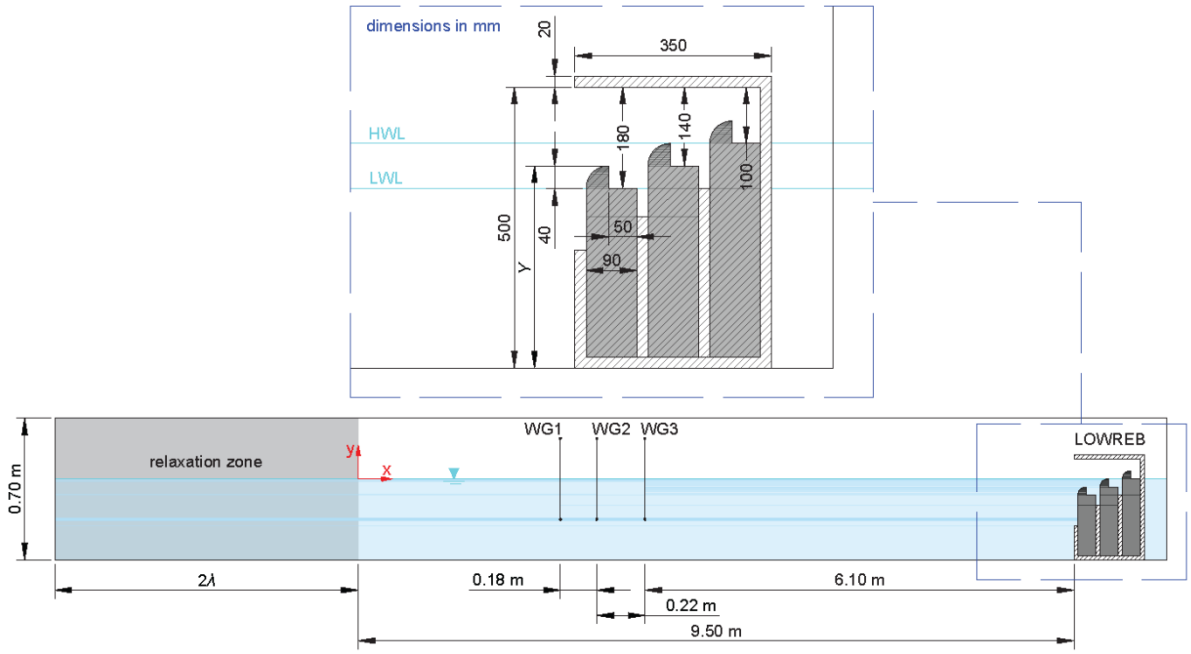

Figure 2. Sketch of the computational domain (not to scale) and detail of the LOWREB model.

Since the LOWREB structure is located at the end of the numerical wave flume and there is no wave transmission beyond it, the outlet relaxation zone was disregarded. Thus, the inlet relaxation zone was the only one implemented (Figure 2). Taking into account that all the energy not dissipated in the LOWREB is reflected towards the inlet boundary of the numerical wave flume, the length of the relaxation zone was set equal to two wavelengths, a length that ensures a correct dissipation even for great amounts of reflected energy (*e.g.*, Hu *et al.*, 2016).

The still water level was set up at a y-coordinate equal to 0. Thus, those cells with a negative y-coordinate were filled with water, i.e., volume fraction α equal to 1, and those cells with a positive y-coordinate were filled with air, *i.e.*, volume fraction α equal to 0. The elevations of the free surface were measured at three positions in front of the structure (Figure 2), preserving the spacing between them used in the experimental tests.

The computational domain was discretized using the OpenFOAM® mesh generation tool *snappyHexMesh*, an algorithm that refines the mesh and adjusts it to fit around a provided geometry using quadratic refinement. Three different regions can be distinguished in the mesh (Figure 3). The first one, the greater, goes from the inlet to the beginning of the transition zone. In this section, a uniform mesh along the x-axis was established. The cell size was determined according to the wavelength in such a way that, at least, there were 50 cells per wavelength (Vanneste and Troch, 2015). Along the y-axis, a non-uniform mesh was established, with a finer sub-mesh region around the free surface, where a cell size of $\Delta y = 5$ mm was implemented. It implies a $H/\Delta y$ ratio greater than 20 for the largest tested waves and greater than or equal to 2 for the smallest ones, which was found to be sufficient in similar applications (Vanneste and Troch, 2015). For the first eight layers of cells near the free surface (both above and below) a cell size of $\Delta y = 10$ mm was set. Finally, a cell size of $\Delta y = 20$ mm was used for the remaining cells of this region.

The second section is the transition zone. It follows the same discretization of the previous section in the *y*-axis. However, along the *x*-axis a variable cell size was established, using a growth rate in which the cell size was reduced slowly providing a smooth transition from the cell size in the propagation section to that in the model section. Finally, the third section of the computational domain is the model testing zone. In this zone, a base cell size of $\Delta x = \Delta y = 20$ mm was used. The cells near the walls of the LOWREB model were refined to easily accommodate the shape of the model. Three levels of refinement and two buffer layers were used in order to achieve a smooth transition between cell sizes. In addition, a refinement box was used both in front and inside the LOWREB model to reduce the cell size to $\Delta x = \Delta z = 5$ mm, which was shown to provide enough detail (*e.g.*, Higuera *et al.*, 2014b). All the cells in this section have an aspect ratio of 1, which was shown to be the best for solving wave breaking (Jacobsen *et al.*, 2012). To achieve a two-dimensional domain, one cell was established in the z direction in the whole domain.

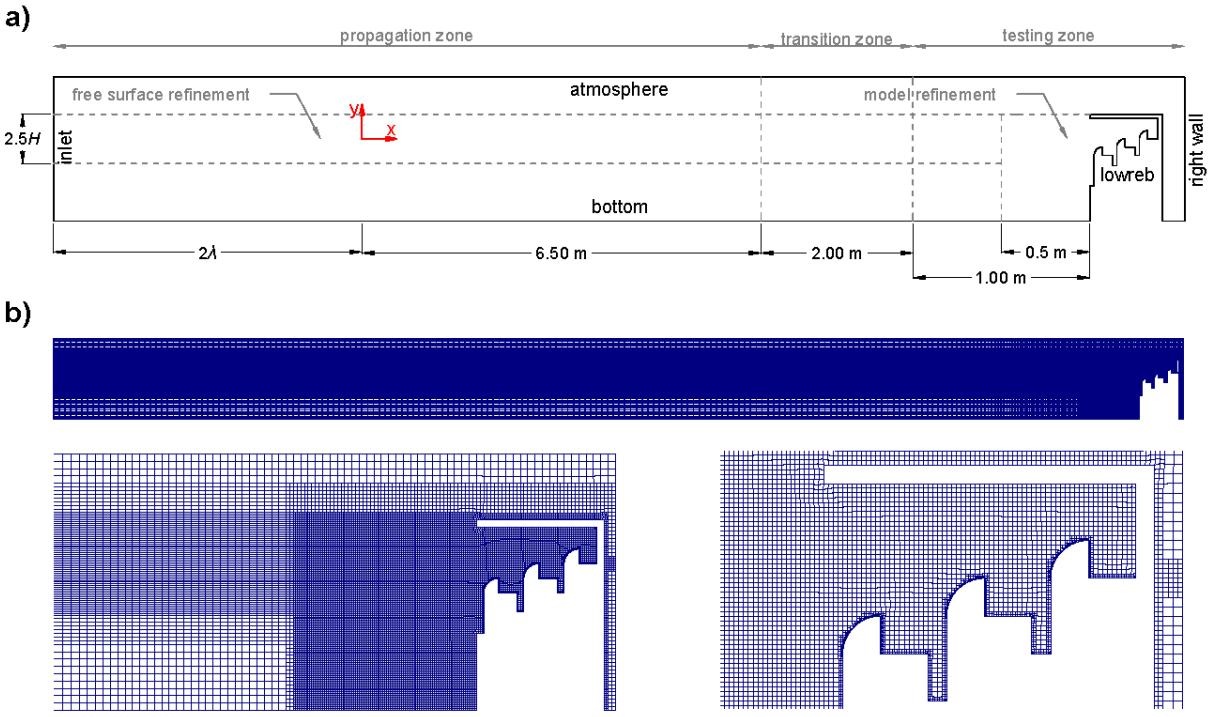

Figure 3. (a) Sketch of the meshing domain with the boundary conditions, where the grey lines inside the geometry indicate the different meshing regions; and (b) general view of the computational mesh of the flume, and detail of the model testing zone and the LOWREB dissipative chambers.

The boundary conditions (Figure 3) were defined as follows. The inlet boundary was set to the *waves2Foam* special wave generating condition both for velocity and volume fraction; pressure and turbulent variables were set to zero normal gradients. For the atmosphere boundary, a fixed total pressure condition was used; the velocity was set using a *pressureInletOutletVelocity* condition, which establishes a zero-gradient condition in case of an outwards flux and calculates the normal velocity on the boundary in the case of an inwards flux; the turbulent variables and the volume fraction were set to an *inletOutlet* condition allowing water to leave and air to enter the domain when needed. The bottom, the right wall and the boundaries of the LOWREB caisson were set as fixed walls with no-slip boundary conditions for velocity, zero gradients for pressure and volume fraction, and wall-functions for k and ε. Finally, given that the computational domain is bi-dimensional, the front and back boundaries were set to *empty*, i.e., the flow field in the direction perpendicular to these boundaries is not solved.

3.3. Testing programme

The testing programme involved two different sets of tests. The objective of the first set was to validate the numerical model. Once validated, the numerical model was used to assess the hydrodynamics of the LOWREB concept. Finally, a second set of tests was conducted covering additional wave conditions in order to better understand the behavior of the LOWREB caisson.

The validation set reproduces the experimental tests carried out with regular waves. Thus, the wave conditions considered were those tested in the physical model, obtained as a combination of three wave heights: 0.11, 0.12 and 0.13 m (5.5, 6.0 and 6.5 m in prototype dimensions, respectively); and three wave periods: 1.41, 1.98 and 2.55 s (10, 14 and 18 s in prototype dimensions, respectively). The tests were carried out for two water depths: low water level (LWL), corresponding to a depth of 0.32 m (16 m in prototype dimensions), and high water level (HWL), corresponding to a depth of 0.40 m (20 m in prototype dimensions). The majority of the cases were generated using Stokes theory, choosing between Stokes first-order and Stokes second-order theory depending on the value of the wave steepness (H/L), being the boundary between linear and Stokes second-order $H/L = 0.04$ (Hedges, 1995). The exception were those cases with a very high Ursell number ($HL^2/d^3 > 50$) in which the cnoidal theory was used. The total simulation time of every case was 60 s.

In the second set of tests the range of studied wave conditions was extended, covering two different situations corresponding to typical applications of the LOWREB caisson: breakwaters and quay-walls. To test the hydrodynamic performance of the LOWREB as a low-reflection breakwater, seven regular wave conditions were considered (Table 1 – conditions 1 to 7). However, port basins are areas protected from the wave action, which means that in these areas wave conditions are less energetic: in general, waves with shorter periods and smaller wave heights are observed. Therefore, to assess the behaviour of the LOWREB in inner quay-walls, six additional less-energetic wave conditions were tested (Table 1 – conditions 8 to 13).

Table 1. Regular wave conditions tested in the second series of numerical model tests.

Wave	Model		Prototype	
condition	H (m)	T (s)	H (m)	T (s)
1	0.12	1.41	6.0	10
2	0.12	1.70	6.0	12
3	0.12	1.98	6.0	14
4	0.06	1.13	3.0	8
5	0.06	1.41	3.0	10
6	0.06	1.70	3.0	12
7	0.06	1.98	3.0	14
8	0.02	0.57	1.0	4
9	0.02	0.85	1.0	6
10	0.02	1.13	1.0	8
11	0.01	0.57	0.5	4
12	0.01	0.85	0.5	6
13	0.01	1.13	0.5	8

The wave conditions of this second set were tested under three different water depths: the LWL and the HWL mentioned above and, in addition, the mean water level (MWL), corresponding to a depth of 0.36 m (18 m in prototype dimensions). Thus, a total number of 39 numerical cases were tested. Both the total simulation time and the criteria for selecting the generation wave theory remain the same of the validation set.

Simulations were carried out in the high performance computing (HPC) center at the Faculty of Engineering of the University of Porto, Portugal (GRID-FEUP). All of them were run in parallel mode with Intel® Xeon® E5-

2640 processors at 2.5 GHz, on four computational cores, which reduced the computational time to approximately 24 hours per case for 60 s of simulation.

The performance of the LOWREB caisson was evaluated based on the reflection coefficients estimated for every wave condition considered. The reflection analysis was carried out using the two-gauge method of Baldock and Simmonds (1999), which allows separating wave trains propagating over an arbitrary 2D bathymetry and is applicable to both regular and irregular waves.

The LOWREB structure, given its geometrical characteristics, may suffer of uplift loads on the horizontal slab at the top (Kisacik *et al.*, 2012a; 2014). Thus, to complement the hydrodynamic analysis of the LOWREB caisson, a preliminary study of the pressure distributions on the horizontal slab was performed. The study of the pressure loads was restricted to the most disadvantageous conditions previously considered, that is, those waves with the higher wave heights (Table 1 – conditions 1 to 3) and under the high water level. To have a high spatial resolution, pressure data was registered at a uniform interval of one data-point each 5 mm. Given the non-repeatability of the breaking wave impact pressures (e.g., Bullock *et al.*, 2007; Kisacik *et al.*, 2012a), pressure measurements were registered for, at least, 10 waves for each test. Data were sampled with a frequency of 1 kHz, a value already used in other studies (e.g., Park *et al.*, 2018).

4. Results

4.1. Numerical model validation

The comparison between the values of the reflection coefficient obtained from physical and numerical modelling is presented in Figure 4. The agreement between both models, physical and numerical, is quite good, with all the cases but one relatively close to the perfect fit line. Thus, without the mentioned exception, all the cases are within the ±10% lines, which are the limits usually assumed when dealing with reflection coefficients (*e.g.*, Jacobsen *et al.*, 2015). The numerical model correctly reproduces the three wave periods, both under LWL and HWL. Although the model tends to slightly underestimate the values of the reflection coefficient for the high period waves (T = 2.55 s), in general, the points are similarly distributed at both sides of the perfect fit line, i.e., there is no strong spurious trends introduced by the numerical model. The erroneous point, which corresponds to a high water level wave condition with a period of T = 1.41 s, can be considered as an outlier, as its behavior is very different from that of the other two cases of the same period, which present a very good agreement with the experimental values.

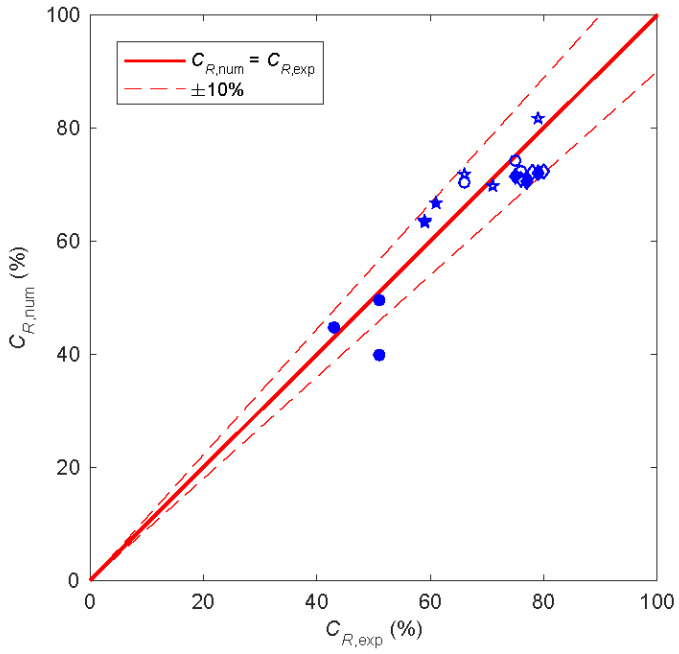

Figure 4. Comparison between the values of the reflection coefficient of the physical and numerical tests (● T = 1.41 s; ★ T = 1.98 s; ♦ T = 2.55; empty symbols: LWL; filled symbols: HWL).

Given the nature of the problem and that the great majority of the values of the reflection coefficient obtained from the numerical modelling match those obtained from physical modelling within an acceptable range (±10%), the numerical model can be considered successfully validated.

4.2. Hydrodynamics of the LOWREB caisson

The previous quantitative validation is qualitatively complemented by comparing the hydrodynamic behavior of the LOWREB caisson on both models, physical and numerical. Thus, the interaction between waves and the LOWREB caisson, under a wave condition of T = 1.41 s and H = 0.11 m, is presented for the physical and numerical models in Figure 5. The snapshots start when the crest of the wave reaches the model and cover an entire wave period.

It can be seen that the agreement between the two models, although not perfect, is quite good. Below are emphasized some events that show the good matching between both models. First, during the wave run-up, the flow impacts the second and third weirs at snapshots 3 and 4, respectively, both on the physical and numerical model (Figure 5). Second, the run-up flow reaches a similar elevation at the entrance of the LOWREB on both models (snapshots 4 and 5). Third, the slope of the free surface inside the LOWREB during the beginning of the discharge stage is approximately the same on both models (snapshots 8, 9 and 10). Fourth, the curved shape of the free surface over the weirs inside the LOWREB (snapshots 10, 11 and 12) is very well reproduced by the numerical model. Finally, the behavior of the incoming waves, which begin the wave run-up stage by the overtopping of the outflow stream, is also well reproduced by the numerical model (snapshot 14).

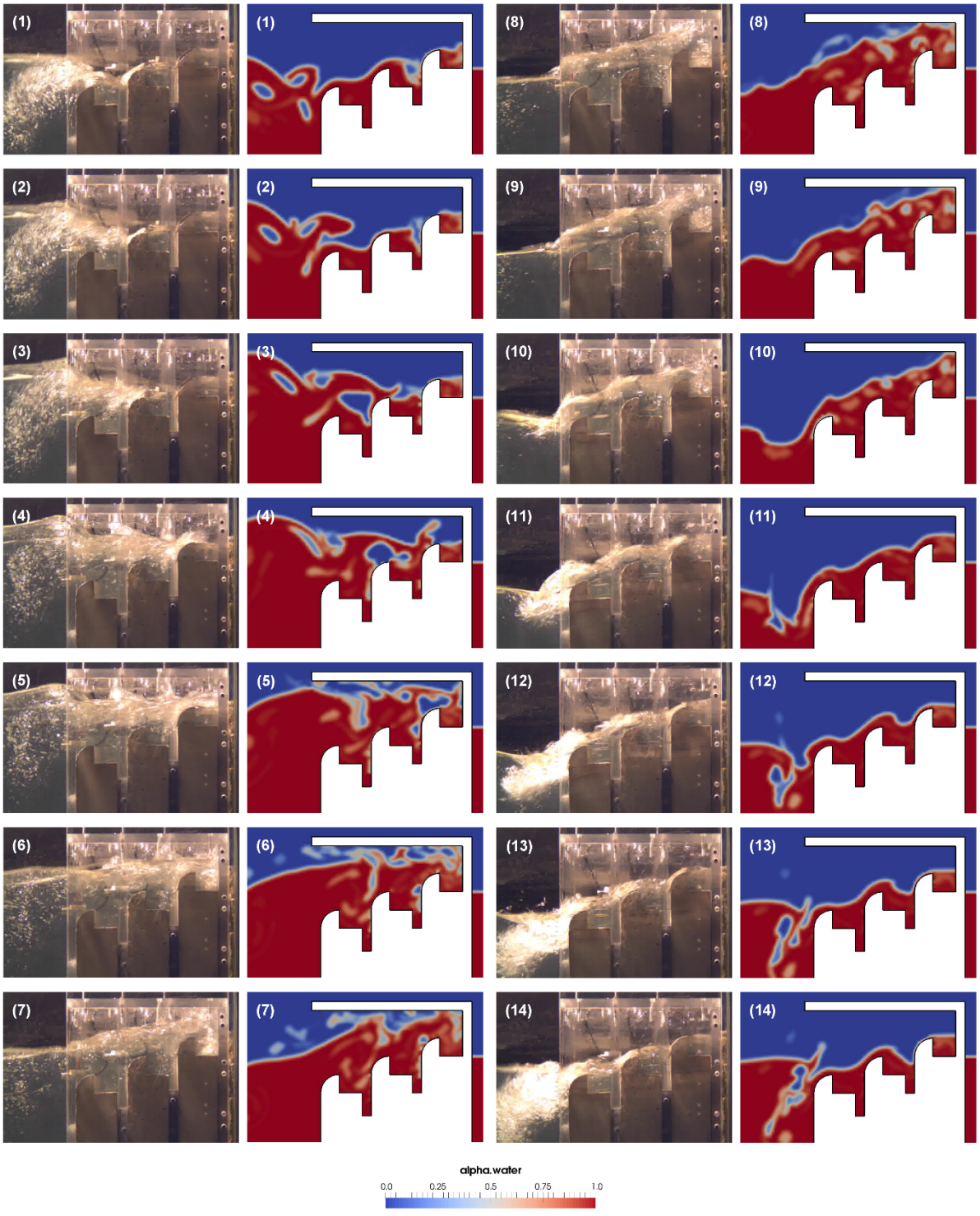

Figure 5. Snapshots of recorded video from the experimental tests and corresponding snapshots from the numerical tests, presenting the wave–LOWREB interaction during an entire wave period under a wave condition of H = 0.11 m, T = 1.41 s and high water level (the time step is 0.10 s, in model time).

On the downside, the intense flow aeration shown in the physical model at the front of the LOWREB, *e.g.*, snapshots 12, 13 and 14 (Figure 5), is not perfectly reproduced in the numerical model, which presents larger air bubbles and lower mixture between air and water phases. This fact can be explained by the 2D nature of the numerical model and, mainly, by the intrinsic characteristics of the VOF method, which assumes the

358 immiscibility of the phases and makes difficult an accurate prediction of air-entrainment. In any case, the
359 hydrodynamic behavior of the numerical model is, in general, in good agreement with that of the experimental
360 model, complementing and reinforcing the validation process.

361 Additionally, the numerical model enables the assessment of other interesting variables for the study of the
362 hydrodynamics of the LOWREB: the velocity fields (Figure 6), the streamlines (Figure 7) and the vorticity fields
363 (Figure 8). To improve the readability of the figures only the fields of the water phase are represented.

364 The analysis of the velocity fields of the LOWREB caisson (Figure 6) shows an acceleration of the flow near the
365 surface when the waves reach the structure (snapshots 1 and 2). Consequently, wave run-up takes place over the
366 weirs at each dissipative chamber. In the process, the run-up flow also impacts the walls of the chambers and the
367 weirs (snapshots 3 and 4). In this way, the run-up energy is dissipated through turbulence and in the impact with
368 the dissipative chamber contours. The splash of the run-up flow takes place when the wave hits the rear wall of
369 the LOWREB caisson (snapshots 5 and 6). At this point, the particle velocity slows down from around 1.5 m/s
370 (in model scale) during the run-up (snapshots 3 and 4) to about 1.0 m/s after the wave impact on the rear wall of
371 the LOWREB caisson (snapshots 6 and 7). The greater velocities (around 1.8 m/s, in model scale) appear during
372 the discharge stage with the outflow stream generated over the crest of the first weir, at the entrance of the
373 LOWREB structure (snapshot 11).

374 In the run-up stage, two main vortices are formed, as can be seen through the streamlines (Figure 7). The first
375 one appears with the approaching of the wave to the LOWREB caisson, at the front of the structure (snapshots 4
376 and 5). The second vortex is formed inside the first dissipative chamber, behind the first weir, and grows with
377 the wave run-up. Furthermore, in addition to these two vortices, a lot of small vortices are formed inside the
378 dissipative chambers. All these vortices are interesting from the operating point of view of the LOWREB as they
379 contribute to increase the energy dissipation of the structure, so diminishing the wave reflection.

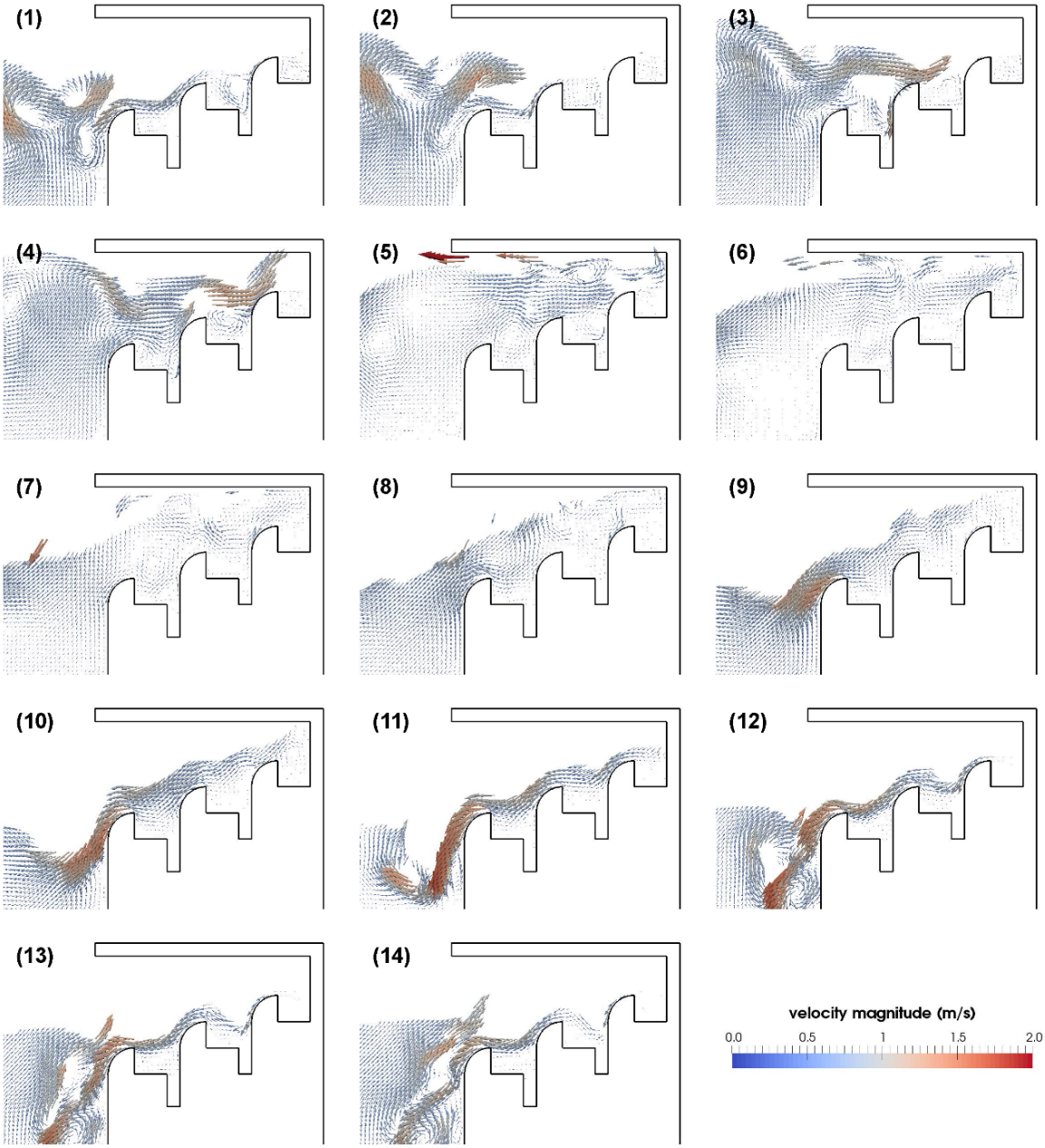

Figure 6. Snapshots of the numerical velocity fields during an entire wave period, under a wave condition of *H* = 0.11 m, *T* = 1.41 s and high water level (the time step is 0.10 s, in model time).

During the return flow, the streamlines present the characteristic curved shaped of the napped flow (snapshots 9 to 14 in Figure 7). Moreover, recirculating vortices are developed in the spaces between the weirs. Thus, in this stage, there are two main events in which energy dissipation takes place: first, when water cascades from one weir to the following one; and second, with the transfer of energy from the outflow stream to the recirculating vortices formed in the dissipative chambers.

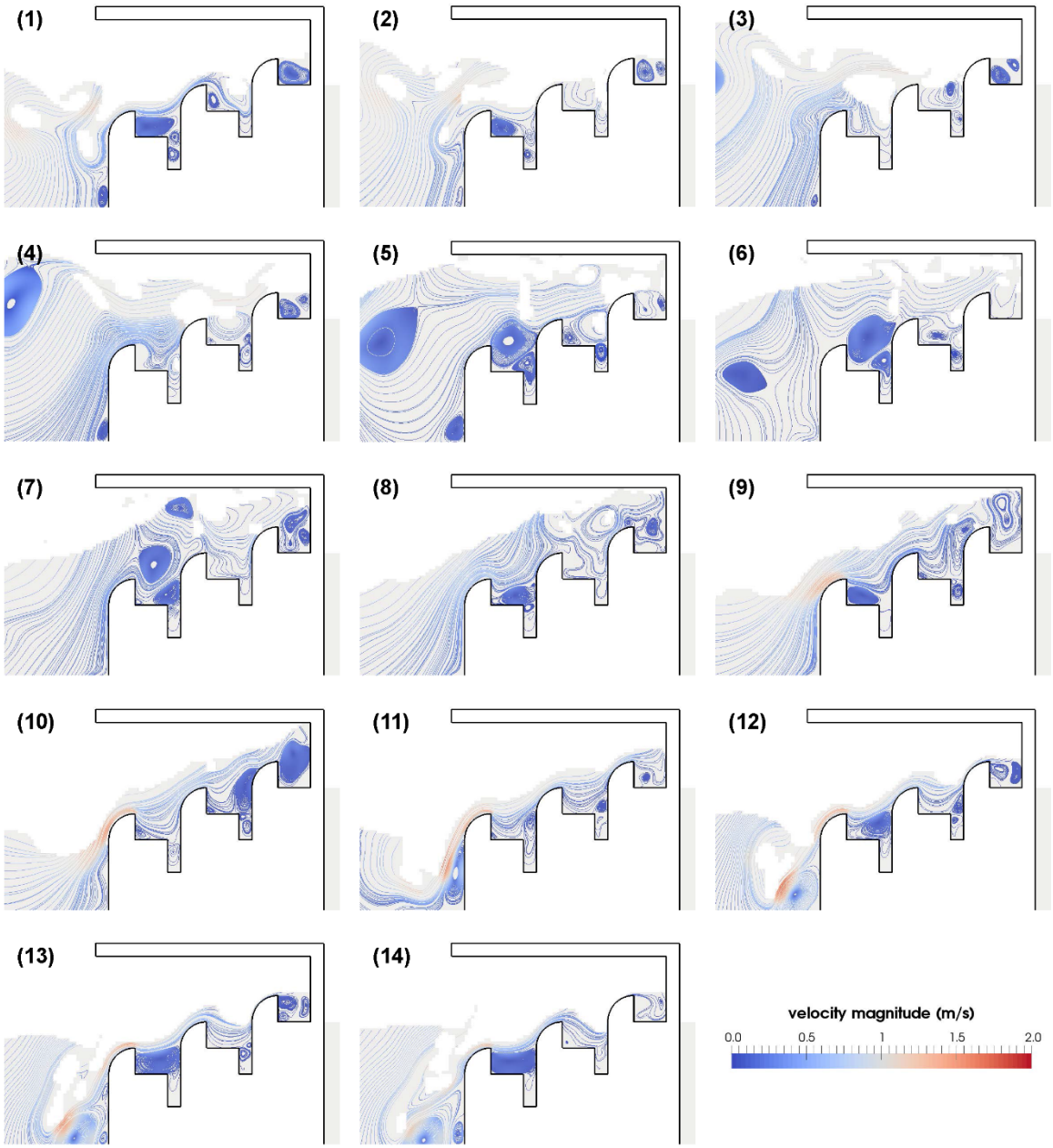

Figure 7. Snapshots of the numerical streamlines during an entire wave period, under a wave condition of *H* = 0.11 m, *T* = 1.41 s and high water level (the time step is 0.10 s, in model time).

As regards vorticity (Figure 8), the greatest values appear, all over the entire wave period, in the regions of contact between the wave flow and the crests of the weirs. The area just at the front of the LOWREB, where the discharge of the high velocity stream outflow is produced, is another remarkable zone of high vorticity (snapshots 11 to 14 in Figure 8); here, a large counterclockwise vortex is formed close to the front wall (snapshot 10 in Figure 7 and Figure 8), grows with the increase of the velocity and detaches from the wall at the end of the wave period (snapshots 12 to 14). Considering the sign of the vorticity, it can be seen that the run-up stage is dominated by negative values, i.e., clockwise rotation (bluish colors of snapshots 1 to 7 in Figure 8), whereas the return flow stage is dominated by positive values, i.e., counterclockwise rotation (yellowish colors of snapshots 8 to 14 in Figure 8).

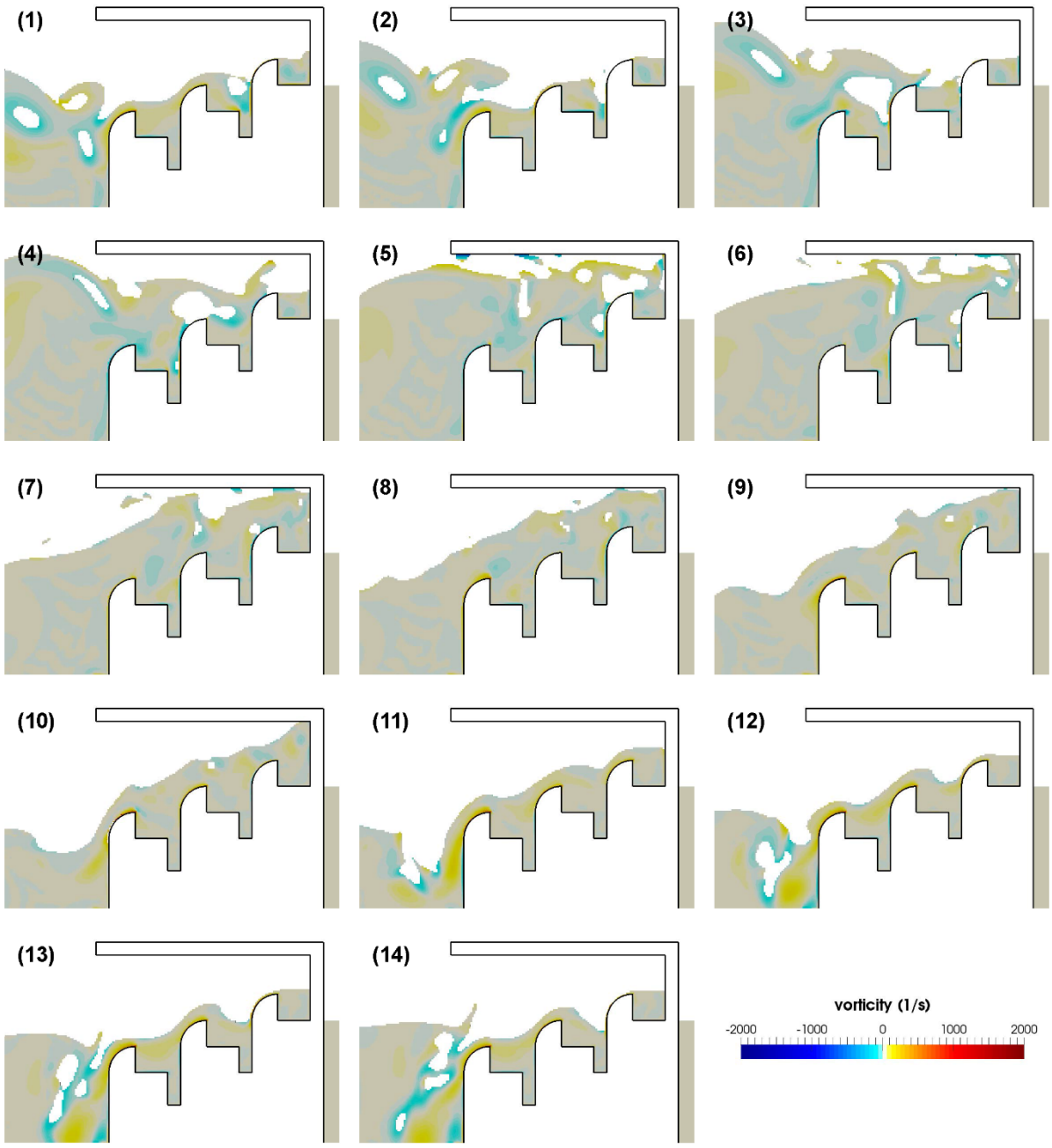

Figure 8. Snapshots of the numerical vorticity fields (component orthogonal to the plane of motion) during an entire wave period, under a wave condition of H = 0.11 m, T = 1.41 s and high water level (the time step is 0.10 s, in model time).

4.3. Performance under extended wave conditions

The analysis of the efficiency of the LOWREB caisson with respect to wave reflection for the extended range of wave conditions tested with the numerical model is presented in Figure 9. The left side of each graph (smaller periods and less-energetic waves) corresponds to the assessment of the LOWREB behavior in inner quay-walls; the right side corresponds to the assessment of the LOWREB as a low-reflection breakwater. It should be noted that the aim of the LOWREB is to reduce the wave reflection; therefore, the lower the reflection coefficient, the better the performance of the LOWREB.

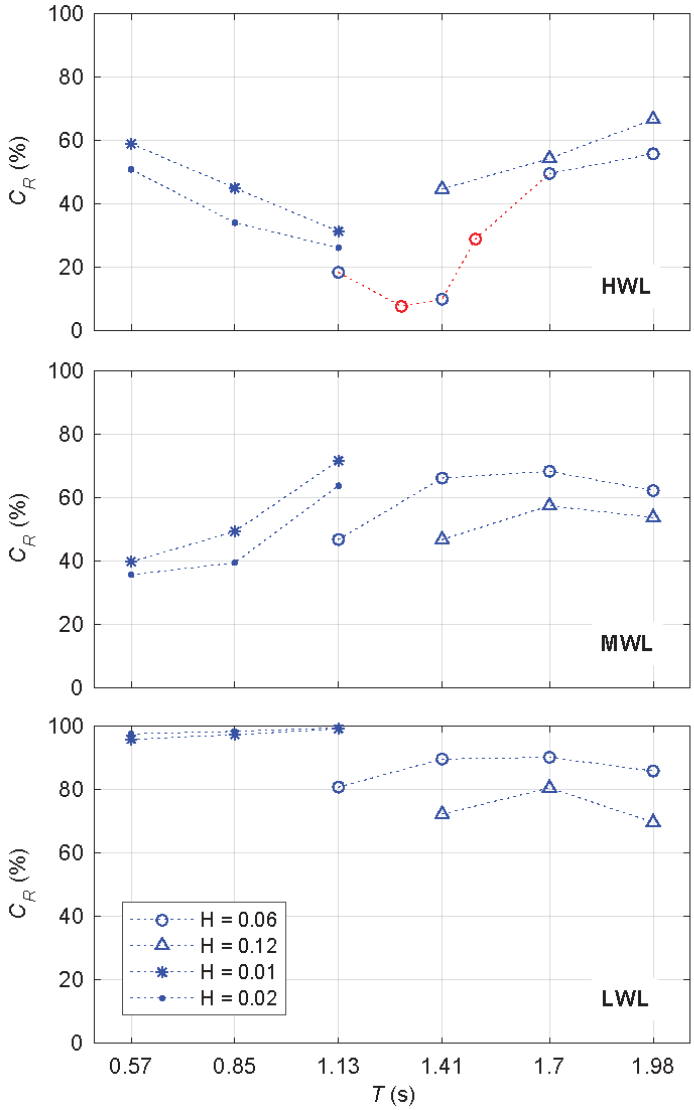

411

412 **Figure 9. Values of the reflection coefficient (C_R) for the different wave conditions tested in the numerical model. Each**
413 **graph corresponds to a different water level: low water level (LWL), mean water level (MWL) and high water level**
414 **(HWL).**

415 Comparing the three graphs in Figure 9, the influence of the water level on the reflection coefficient is evident;
416 thus, there are differences from up to 80 percentage points in the values of the reflection coefficient between low
417 and high water levels for the same wave condition (*e.g.*, $H = 0.06$ m, $T = 1.41$ s). Overall, the LOWREB
418 achieves the best performance for the high water level condition, for which the values of the reflection
419 coefficient for the great majority of the wave conditions are well below 60%. The performance of the LOWREB
420 for the mean water level is also satisfactory, with all the values of the reflection coefficient below 70% and most
421 of them in the range 30%-60%. At low water level, the performance of the LOWREB is not good: all the values
422 of the reflection coefficient are above 70%. Therefore, the geometry of the LOWREB caisson is not optimized
423 for the low water level. The strong influence of the water level on the LOWREB performance must be related to
424 the accessibility of the wave to the LOWREB dissipative chambers, which is more difficult under the low water
425 level. In fact, in this situation waves hardly overtop the weir of the third dissipative chamber (the higher one). A
426 similar conclusion was found in the experimental model tests (Ciocan *et al.*, 2017).

Paying attention to the graph of the low water level (Figure 9 – LWL), the values of the reflection coefficient for the two smaller wave heights (H = 0.01 and 0.02 m) are near 100%, *i.e.*, the LOWREB performs as a vertical wall. The reason is that the waves are not able to overtop even the first weir (*e.g.*, Figure 10). When the wave height increases, the LOWREB starts to perform better. In fact, for this water level, the wave height is the variable that most influence the reflection coefficient: the higher the wave height, the lower the reflection coefficient. The influence of the wave period is comparatively smaller.

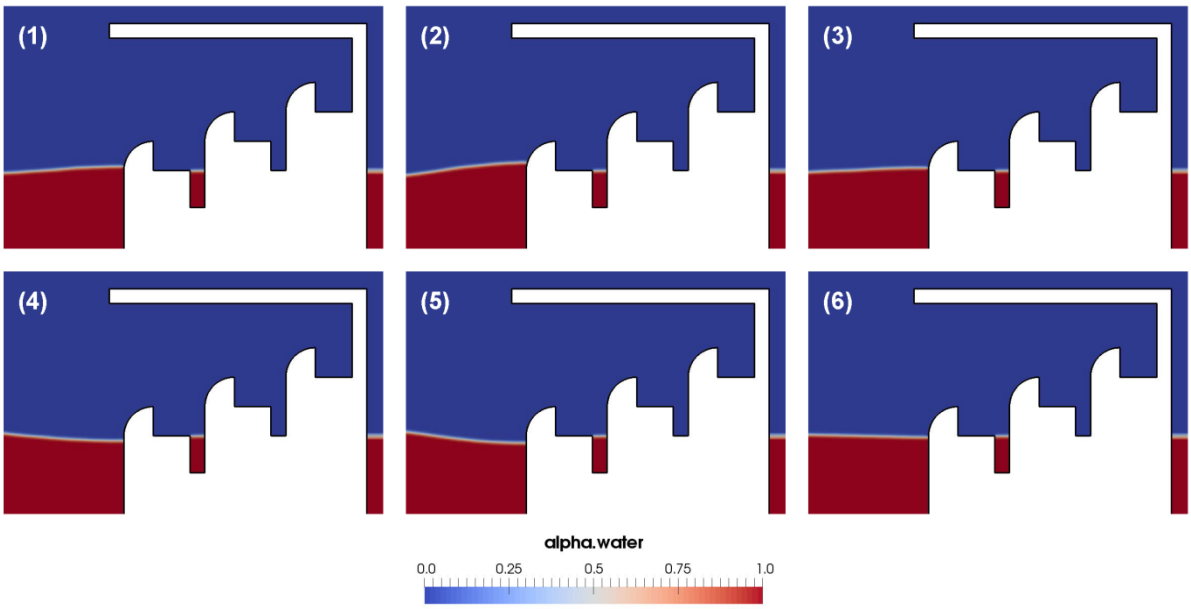

Figure 10. Snapshots from the numerical tests, presenting the wave–LOWREB interaction during an entire wave period under a wave condition of H = 0.02 m, T = 0.57 s and low water level (the time step is 0.10 s, in model time).

A different situation takes place for the high water level condition (Figure 9 – HWL). For HWL, wave period is clearly the most important variable on the LOWREB performance. For a given wave height, variations in the wave period produce changes in the values of the reflection coefficient of more than 20 percentage points. Particularly interesting are the results of H = 0.06 m: there is a wave period (T = 1.41 s) for which the energy dissipation is maximum ($C_R \approx 10\%$). What is more, the LOWREB improves its performance (lower values of the reflection coefficient) when the wave period gets close to this optimum period for the four studied wave heights. This behavior, however, is not reproduced for the mean water level condition (Figure 9 – MWL): there is no optimum period, at least, in the range of studied wave conditions. Therefore, the performance of the LOWREB is highly influenced by the combined effect of wave period and water level.

With the aim of confirming the exceptional performance achieved by the LOWREB at high water level for a wave condition of H = 0.06 m and T = 1.41 s, two additional cases were tested, maintaining the wave height and introducing small variations in the wave period (T = 1.30 and 1.50 s). The values of the reflection coefficient for this additional wave conditions are presented in red in Figure 9 – HWL. The performance of the LOWREB is in accordance with the previous results. Thus, a well-defined trend towards an optimum period in the vicinity of T = 1.30-1.41 s can be observed. Similar values of the reflection coefficient (about 10%) were also found for optimum conditions in other low-reflection structures (*e.g.*, Faraci *et al.*, 2014).

Special attention must be payed to the low-energy wave conditions. For the MWL, the values of the reflection coefficient increase when the wave period increases. Nevertheless, for the HWL, the values of the reflection

coefficient decrease when wave period increases. At MWL, the low-energy waves are not able to overtop the crest of the second weir, so only one of the three dissipative chambers of the LOWREB is effectively working. At HWL, the low-energy waves do overtop the crest of the second weir and two dissipative chambers work. This situation improves the performance of the LOWREB for the wave period of T = 1.13 s and worsen it for T = 0.57 s; for an intermediate period (T = 0.85 s) the performance of the LOWREB is the same for both water levels. Again, it is shown that the LOWREB efficiency is highly influenced by the combined effect of wave period and water level.

As regards wave height, in general, the reflection coefficient decreases when the wave height increases. This is true for low and mean water levels, and for the less-energetic wave conditions of the high water level. However, at high water level this trend switches under the more-energetic wave conditions (H = 0.06 and 0.12 m); in this case, the highest wave height corresponds to the lowest performance of the LOWREB. In this situation, probably, the total height of the LOWREB structure is not enough to correctly dissipate the incident wave energy; in fact, for the high water level, the largest waves are close to overtop the structure (*e.g.*, Figure 5).

To better characterize the behavior of the LOWREB, the values of the reflection coefficient are presented versus the relative crest freeboard, $R^* = Y/(H+h)$, in Figure 11, for the entire set of tested wave conditions. This non-dimensional parameter is usually defined as the ratio of the height of the structure over the water level (*i.e.*, the crest freeboard) to the wave height; however, in this case, to prevent the numerator from being equal to zero, the water depth was added in the denominator rather than subtracted from the chamber height (see Figure 2 for definition of the chamber height, Y). Following the subdivision established in Section 3.3, the dataset was divided into high-energetic waves (Table 1 – conditions 1 to 7) and low-energetic waves (Table 1 – conditions 8 to 13). In general, the lower the relative crest freeboard, the lower the values of the reflection coefficient. This shows that in order to reduce the values of the reflection coefficient, the crest freeboard should be smaller than the wave height, which is directly related to the capability of the waves to overtop the weirs and reach the dissipative chambers. The slope of the fitted line is greater for the low-energetic waves, which means that the influence of the relative crest freeboard on the performance of the LOWREB is higher under these conditions characterized by smaller wave heights. An appropriate design of the LOWREB should ensure values of the relative crest freeboard never greater than one and, preferably, below 0.9 for low-energetic waves and 0.8 for high-energetic waves.

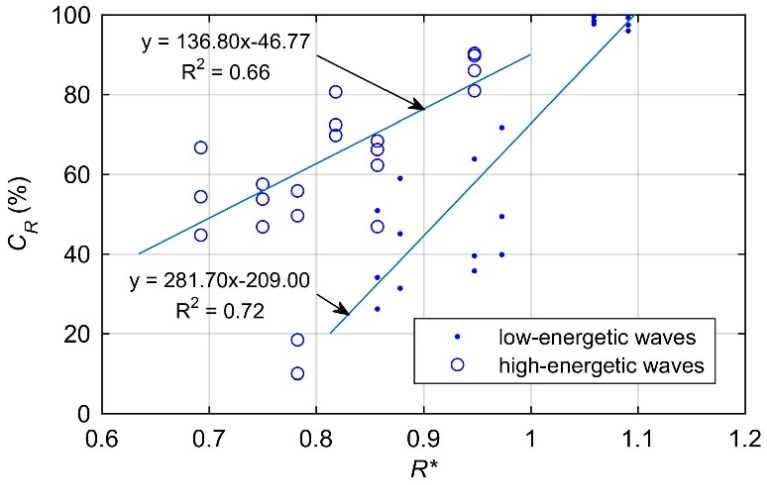

Figure 11. Values of the reflection coefficient (C_R) as a function of the relative crest freeboard (R^*).

Other non-dimensional parameters usually employed in the study of conventional non-reflective structures, *e.g.*, the relative dissipation chamber width (ratio of the chamber width to the wavelength), are hardly applicable to the LOWREB concept due to the presence of the inner weirs and the variable water depths inside the dissipative chambers, which modify the effective dissipation chamber width, making the analysis highly complex. Thus, although the performance of the LOWREB is highly influenced by the wave period, no non-dimensional parameter was found which related this influence to any other of the investigated variables in a clear manner.

4.4. Pressures on the horizontal slab

The time-varying spatial pressure distributions for one of the tested cases are presented in Figure 12, in which the normalized time (t/T) is represented along the y-axis, the x-axis shows the normalized position along the horizontal slab at the top of the LOWREB structure (x/x_L), and the normalized pressure is represented in the z-axis. For readability, only three consecutive wave impacts are presented. It can be seen that the impact behavior varies from one wave to another, as initially expected. The higher pressures are located on the first half of the slab, with the maximum pressure at the corner near the vertical wall. Further away from the first half of the slab, pressure diminish substantially.

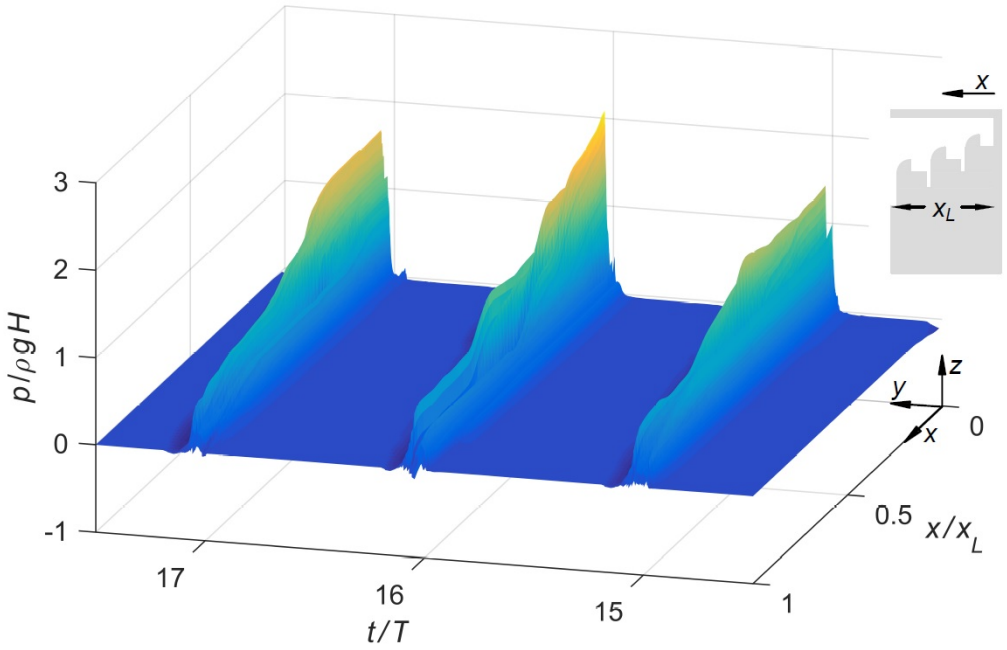

Figure 12. Time-varying spatial pressure profiles on the horizontal slab for three consecutive wave impacts, under a wave condition of H = 0.12 m, T = 1.98 s and for the high water level.

To better analyze the most disadvantageous conditions, the normalized instantaneous pressure profiles at the time of maximum pressures are presented in Figure 13, for the three considered cases (Table 1 – conditions 1 to 3). The pressure profiles of the three conditions are similar: a near-triangular shape with the maximum pressure at the corner of the structure, reducing progressively towards the tip of the horizontal slab. However, the differences both in magnitude and in affected length of the slab are noticeable. Thus, for the two smaller periods, T = 1.41 and 1.70 s (Figure 13 – A and B), the wave impact is located in the first fifth of the horizontal slab ($0 < x/x_L < 0.2$). For the larger period, T = 1.98 s (Figure 13 – C), the wave impact affects, approximately, four fifths of the total length of the slab ($0 < x/x_L < 0.8$). This larger period is also that which presents the higher values of the reflection coefficient of the three here evaluated (Figure 9 – HWL). This indicates that the higher

pressures take place for wave conditions with the higher reflections, i.e., those for which the hydraulic efficiency of the LOWREB is low. In any case, the values of the maximum pressure are not very high, $p_{max} < 3\rho gH$. In previous studies dealing with wave impacts on vertical structures with horizontal slabs, values of the maximum pressure well above $50\rho gH$ were found (Kisacik *et al.*, 2012a; 2012b). The particular geometrical shape of the LOWREB, which forces wave breaking and enhances energy dissipation, is surely related to these comparatively lower pressures. This is a good result, in the sense that the integrity of the caisson seems not to be particularly threatened because of the wave impacts, nor operating as a breakwater nor consequently as a quay-wall.

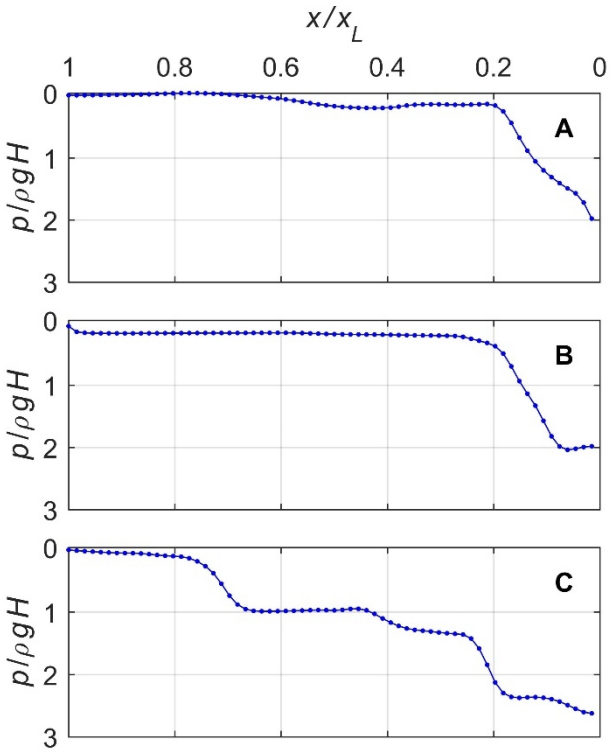

Figure 13. Normalized instantaneous pressure profiles at the time of maximum pressures: (A) *H* = 0.12 m, *T* = 1.41 s; (B) *H* = 0.12 m, *T* = 1.70 s; and (C) *H* = 0.12 m, *T* = 1.98 s.

Finally, it should be noted that this pressure analysis is preliminary and despite showing a general representation of the behavior of the structure when facing wave impacts, demands a cautious evaluation of the results. In fact, an in-depth study of the problem requires the improvement of some points, e.g., a higher sampling frequency and a higher number of analyzed waves for reducing the uncertainty associated with non-repeatability. Furthermore, a comparison with experimental pressure measurements would be recommended to confirm the numerical model results. This is a topic that deserves further study.

5. Conclusions

In this work, the OpenFOAM® CFD package in combination with the *waves2Foam* wave generation toolbox was used to implement a RANS-VOF numerical model of the LOWREB concept. The model, once validated using the results from experimental tests, was applied, first, to carry out an in-depth study of the hydrodynamics of the LOWREB and, second, to assess its performance under an extended range of wave conditions, covering in this way the main uses of the LOWREB caisson concept: external caisson breakwater or inner low reflective quay-wall.

The validation was carried out following a two-stage approach. First, the values of the reflection coefficient calculated from the numerical model simulations were compared with those from experimental modelling. A good agreement was found: excepting one outlier, all the cases are within the ±10% error interval. After that, a qualitative validation was made by comparing the wave-structure interaction on both models, physical and numerical, under a given wave condition. A series of characteristic events were analyzed, showing a good matching between the physical and numerical models.

The analysis of the LOWREB hydrodynamics, for which the velocity fields, the streamlines and the vorticity fields were evaluated, enabled the detailed characterization of the energy dissipation events that take place in the wave-LOWREB interaction. These are, mainly, the impacts of the wave run-up flow with the weirs of the dissipative chambers during the wave run-up stage, and the napped flow (the outflow stream that cascades from one weir to another) during the spill-out stage. These events contribute to the formation of numerous vortices along the entire wave period cycle, not only inside the dissipative chambers but also in front of the LOWREB structure. All these mechanisms increase turbulence and, in this way, energy dissipation through viscous shear stress.

The performance of the LOWREB, characterized based on the values of the reflection coefficient, was found to be highly influenced by the combined effect of wave period and water level. The influence of the wave height although comparatively lower, is not negligible; in general, a higher wave height contributes to improve the energy dissipation. Overall, the LOWREB achieves its best performance for the high water level condition, with all the values of the reflection coefficient below 70% and most of them in the range 30%-60%. In this situation, the existence of an optimum period (1.13 s < T_{opt} <1.50 s) which maximizes the energy dissipation of the device (a minimum $C_R \approx 10\%$ was obtained for $H = 0.06$ m) was proven. Although this fact suggests that there could be an optimum wave period for a given wave height such that the energy dissipation is maximum, this optimum period was only found at the high water level, so further investigations must be done in this direction. The performance for the mean water level was also good (30% < C_R < 70%), in particular, for the less-energetic wave conditions of shorter period, under which the LOWREB improves the performance achieved at high water level. On the contrary, the performance at low water level was found to be poor for the entire range of wave conditions (C_R > 70%). It is associated with the difficulties that waves have, at this water level, to overtop the weirs and enter the dissipative chambers. To overcome this situation, the LOWREB must be designed to have a relative crest freeboard (R^*) below one. Finally, the analysis of the pressure distributions on the horizontal slab of the LOWREB showed that the integrity of the device is not particularly threatened because of the wave impacts.

To sum up, in this work the hydrodynamic performance of the LOWREB caisson was successfully assessed by means of a RANS-VOF numerical model. The results were promising, with values of the reflection coefficient below 70% for the entire range of wave conditions tested at mean and high water levels. Therefore, the LOWREB concept was shown to be an appropriate low-reflection solution both for breakwaters and quay-walls. Future work should include the development of geometry modifications to ensure a better performance of the LOWREB caisson at lower water levels.

Acknowledgements

During this work I. López was supported by the postdoctoral grant ED481B 2016/125-0 of the 'Programa de Axudas á etapa posdoutoral da Xunta de Galicia (Consellería de Cultura, Educación e Ordenación Universitaria)'.

References

[1] Altomare, C., Gironella, X., 2014. An experimental study on scale effects in wave reflection of low-reflective quay walls with internal rubble mound for regular and random waves. Coast. Eng. 90, 51–63. doi: 10.1016/j.coastaleng.2014.04.002.

[2] Baldock, T.E., Simmonds, D.J., 1999. Separation of incident and reflected waves over sloping bathymetry. Coastal Engineering, 38 (3), 167-176. doi: 10.1016/S0378-3839(99)00046-0.

[3] Berenguer, J.M., Arana, M. (2002). Pieza artificial BARA para la construcción de diques, muelles y riberas de baja reflectividad (BARA artificial block for the construction of breakwaters, quays walls and banks of low reflectivity). Berenguer Ingenieros S.I, Tenerife, Spain [in Spanish].

[4] Bergmann, H., Oumeraci, H., 2001. Wave Loads on Perforated Caisson Breakwaters, in: Coastal Engineering 2000. American Society of Civil Engineers, pp. 1622–1635.

[5] Bottin, R.R., Jr. ed. (1976). Igloo wave absorber tests for Port Washington Harbor WI. Hydraulic Model Investigation. Miscellaneous Paper H-76-22. U.S. Army Engineer Waterways Experiment Station, Vicksburg MS.

[6] Bullock, G.N., Obhrai, C., Peregrine, D.H., Bredmose, H., 2007. Violent breaking wave impacts. Part 1: results from large-scale regular wave tests on vertical and sloping walls. Coastal Engineering 54 (8), 602–617. https://doi.org/10.1016/j.coastaleng.2006.12.002.

[7] Chen, X., Li, Y., Sun, D., 2002. Regular waves acting on double-layered perforated caissons. Presented at the The Twelfth International Offshore and Polar Engineering Conference, International Society of Offshore and Polar Engineers, Kitakyushu, Japan, pp. 736–743.

[8] Ciocan, C.-S., Taveira-Pinto, F., das Neves, L., Rosa-Santos, P., 2017. "Experimental study of the hydraulic efficiency of a novel perforated-wall caisson concept, the LOWREB", Coastal Engineering (Elsevier). ISSN: 0378-3839, Vol. 126, pp. 69-80, doi: 10.1016/j.coastaleng.2017.06.001.

[9] Cho, I.H., Kim, M.H., 2008. Wave absorbing system using inclined perforated plates. J. Fluid Mech. 608, 1–20.

[10] del Jesus, M., Lara, J., Losada, I., 2012. Three-dimensional interaction of waves and porous coastal structures. Coastal Engineering, 64:57-72, ISSN 0378-3839, doi: 10.1016/j.coastaleng.2012.01.008.

[11] Faraci, C.; Scandura, P.; Foti, E., 2015. Reflection of Sea Waves by Combined Caissons. Journal of Waterway, Port, Coastal, and Ocean Engineering, 141 (2), 04014036. doi: 10.1061/(ASCE)WW.1943-5460.0000275

[12] Fugazza, M., Natale, L., 1992. Hydraulic Design of Perforated Breakwaters. J. Waterw. Port Coast. Ocean Eng. 118, 1–14. doi:10.1061/(ASCE)0733-950X(1992)118:1(1)

[13] Garrido, J.M., Medina, J.R., 2012. New neural network-derived empirical formulas for estimating wave reflection on Jarlan-type breakwaters. Coastal Engineering. 62, 9–18. doi: 10.1016/j.coastaleng.2011.12.003.

[14] Hedges, T., 1995. Regions of validity of analytical wave theories. Proceedings of the Institution of Civil Engineers - Water Maritime and Energy, 112 (2), 111-114. doi:10.1680/iwtme.1995.27656.

[15] Higuera P., Lara, J., Losada, I., 2013. Simulating coastal engineering processes with OpenFOAM®, Coastal Engineering, 71:119-134, ISSN 0378-3839, doi:10.1016/j.coastaleng.2012.06.002.

[16] Higuera, P., Lara, J.L., Losada, I.J., 2014a. Three-dimensional interaction of waves and porous coastal structures using OpenFOAM®. Part I: Formulation and validation. Coast. Eng. 83, 243–258. doi:10.1016/j.coastaleng.2013.08.010.

[17] Higuera, P., Lara, J.L., Losada, I.J., 2014b. Three-dimensional interaction of waves and porous coastal structures using OpenFOAM®. Part II: Application. Coast. Eng. 83, 259–270. doi:10.1016/j.coastaleng.2013.09.002.

[18] Higuera, P., Losada, I., Lara, J., 2015. Three-dimensional numerical wave generation with moving boundaries, Coastal Engineering, 101, 35-47, ISSN 0378-3839, doi:10.1016/j.coastaleng.2015.04.003.

[19] Hirt, C.W., Nichols, B.D., 1981. Volume of Fluid (VoF) method for the dynamics of free boundaries, J. Comput. Phys. 39, 201–225. doi: 10.1016/0021-9991(81)90145-5.

[20] Hu, H., Wang, K.-H., Williams, A.N. (2002). Wave motion over a breakwater system of a horizontal plate and a vertical porous wall. Ocean Eng. 29(4), 373-386, doi: 10.1016/S0029-8018(01)00029-4.

[21] Hu, Z.Z., Greaves, D., Raby, A., 2016. Numerical wave tank study of extreme waves and wave-structure interaction using OpenFoam®, Ocean Engineering 126, 329-342. doi: 10.1016/j.oceaneng.2016.09.017

[22] Huang, Z., 2006. A method to study interactions between narrow-banded random waves and multi-chamber perforated structures. Acta Mech. Sin. 22(4), 285–292. doi:10.1007/s10409-006-0021-x.

[23] Huang, Z., Li, Y., Liu, Y., 2011. Hydraulic performance and wave loadings of perforated/slotted coastal structures: A review. Ocean Eng. 38, 1031–1053. doi:10.1016/j.oceaneng.2011.03.002

[24] Ijima, T., Tanaka, E., Okuzono, H. (1976). Permeable seawall with reservoir and the use of "Warock". Coastal Eng. 151, 2623–2642.

[25] Isaacson, M., Baldwin, J., Allyn, N., Cowdell, S. (2000). Wave interactions with perforated breakwater. J. Wway., Port, Coastal, and Ocean Eng. 126(5), 229–235.

[26] Jacobsen, N.G., Fuhrman, D.R., Fredsøe, J., 2012. A wave generation toolbox for the opensource CFD library: OpenFoam. Int. J. Numer. Methods Fluid 70 (9), 1073–1088. doi: 10.1002/fld.2726

[27] Jacobsen, N.G., van Gent, M.R.A., Wolters, G., 2015. Numerical analysis of the interaction of irregular waves with two dimensional permeable coastal structures. Coastal Engineering, 102, 13–29.

[28] Jarlan, G.E., 1961. A perforated vertical breakwater (No. 486, Vol. 41). The Dock and Harbour Authority, London, UK.

[29] Jasak H. Error analysis and estimation for the finite volume method with applications to fluid flows. PhD Thesis, Imperical College of Science, Technology and Medicine, June 1996.

[30] Jensen, B., Jacobsen, N., Christensen, E., 2014. Investigations on the porous media equations and resistance coefficients for coastal structures. Coastal Engineering, 84, 56-72, ISSN 0378-3839, doi:10.1016/j.coastaleng.2013.11.004.

[31] Kisacik, D., Troch, P., Van Bogaert, P., 2012a. Description of loading conditions due to violent wave impacts on a vertical structure with an overhanging horizontal cantilever slab. Coastal Engineering 60 (1), 201-226. http://dx.doi.org/10.1016/j.coastaleng.2011.10.001

[32] Kisacik, D., Troch, P., Van Bogaert, P., 2012b. Experimental study of violent wave impact on a vertical structure with an overhanging horizontal cantilever slab. Ocean Engineering 49, 1-15. http://dx.doi.org/10.1016/j.oceaneng.2012.04.010

[33] Kisacik, D., Troch, P., Van Bogaert, P., Caspeele, R., 2014. Investigation of uplift impact forces on a vertical wall with an overhanging horizontal cantilever slab. Coastal Engineering 90, 12-22. http://dx.doi.org/10.1016/j.coastaleng.2014.04.011.

[34] Lara, J. L., del Jesus, M., Losada, I.J., 2012. Three-dimensional interaction of waves and porous coastal structures, Coastal Engineering, 64, 26-46, ISSN 0378-3839, doi:10.1016/j.coastaleng.2012.01.009.

[35] Lee, K.-H, Bae, J.-H., Kim S.-G., Kim, D.-S., 2017. Three-dimensional Simulation of Wave Reflection and Pressure Acting on Circular Perforated Caisson Breakwater by OLAFOAM. Journal of Korean Society of Coastal and Ocean Engineers 29(6), pp. 286-304, ISSN 2288-2227. doi:10.9765/KSCOE.2017.29.6.286.

[36] Li Y.C., Dong G.H., Liu H.J. and Sun D.P. (2003). The reflection of oblique incident waves by breakwaters with double-layered perforated wall. *Coast. Eng.* 50: 47–60 DOI 10.1016/j.coastaleng.2003.08.001.

[37] Lin, Y.H., Chen, J.F., Lu, P.Y., 2017. A CFD model for simulating wave run-ups and wave loads in case of different wind turbine foundations influenced by nonlinear waves, Ocean Engineering, 129, 428-440. doi:10.1016/j.oceaneng.2016.10.050.

[38] Liu, Y., Li, Y., Teng, B., 2007.Wave interaction with a new type perforated breakwater. Acta Mechanica Sinica 23(4), 351- 358, doi: 10.1007/s10409-007-0086-1.

[39] Liu, Y., Li, Y., Teng, B., Jiang, J., Ma, B., 2008. Total horizontal and vertical forces of irregular waves on partially perforated caisson breakwaters, Coastal Engineering, 55:6, 537-552, ISSN 0378-3839, doi:10.1016/j.coastaleng.2008.02.005.

[40] Liu, Y., Faraci, C., 2014.Analysis of orthogonal wave reflection by a caisson with open front chamber filled with sloping rubble mound, Coastal Engineering, 91, 2014, 151-163, ISSN 0378-3839, doi:10.1016/j.coastaleng.2014.05.002.

[41] López, M., Iglesias, G., 2014. Long wave effects on a vessel at berth. *Applied Ocean Research*. 47, 63-72, ISSN 0141-1187, doi: 10.1016/j.apor.2014.03.008.

[42] López, I., López, M., Iglesias, G., 2015. Artificial neural networks applied to port operability assessment. *Ocean Engineering*, 109, 298-308, ISSN 0029-8018, doi:10.1016/j.oceaneng.2015.09.016.

[43] López, I., Pereiras, B., Castro, F., Iglesias, G., 2014. Optimisation of turbine-induced damping for an OWC wave energy converter using a RANS–VOF numerical model. Applied Energy 127: 105–114.

[44] OpenFOAM®, OpenFOAM-4.1, 2017. ⟨http://www.openfoam.org/⟩.

[45] Park, H., Do, T., Tomiczek, T., Cox, D.T., van de Lindt, J.W., 2018. Numerical modeling of non-breaking, impulsive breaking, and broken wave interaction with elevated coastal structures: Laboratory validation and inter-model comparisons. Ocean Engineering 158, 78-98. https://doi.org/10.1016/j.oceaneng.2018.03.088.

[46] Pinto, S.I., 2012. Estrutura portuárias verticais perfuradas (MSc dissertation). Universidade do Porto - Faculdade de Engenharia, Porto, Portugal [Reference in Portuguese].

[47] Rosa-Santos, P.; Taveira-Pinto, F.; 2013. "Experimental study of solutions to reduce downtime problems in ocean facing ports: the Port of Leixões, Portugal, case study", Journal of Applied Water Engineering and Research (Taylor and Francis), ISSN: 2324-9676 (Online), Vol. 1. No. 1, pp. 80-90, doi: 10.1080/23249676.2013.831590.

[48] Rosa-Santos, P., Taveira-Pinto, F., Veloso-Gomes, F., 2014. Experimental evaluation of the tension mooring effect on the response of moored ships. Coast. Eng. 85, 60–71. doi:10.1016/j.coastaleng.2013.11.012.

[49] Song, H.,Tao,L. (2007). Short-crested wave interaction with a concentric porous cylindrical structure. Applied Ocean Res. 29(4), 199–209, doi: 10.1016/j.apor.2008.01.001. ISSN 0141-1187.

[50] Suh, K.-D., Park, J.K., Park, W.S., 2006. Wave reflection from partially perforated-wall caisson breakwater. Ocean Eng. 33, 264–280. doi:10.1016/j.oceaneng.2004.11.015

[51] Taveira-Pinto, F., Rosa-Santos, P., Veloso-Gomes, F., Lopes, H., 2011. Efficiency analysis to reflection of a new quay wall type. *Journal of Hydraulic Research*. 49, 539–546. doi:10.1080/00221686.2011.574378.

[52] Theocharis, I., Anastasaki, E.N., Moutzouris, C.I., Giantsi, T., 2011. A new wave absorbing quay-wall for wave height reduction in a harbor basin. Ocean Eng. 38, 1967–1978. doi:10.1016/j.oceaneng.2011.09.020.

[53] Vanneste, D., Troch, P., 2015. 2D numerical simulation of large-scale physical model tests of wave interaction with a rubble-mound breakwater. Coastal Engineering, 103, 22–41. doi:10.1016/j.coastaleng.2015.05.008.

[54] Williams, A.N., Mansour, A.-E.M., Lee, H.S., 2000. Simplified analytical solutions for wave interaction with absorbing-type caisson breakwaters. Ocean Eng. 27, 1231–1248. doi:10.1016/S0029-8018(99)00045-1.

[55] Wu, Y.-T., Yeh, C.-L., Hsiao, S.-C., 2014.Three-dimensional numerical simulation on the interaction of solitary waves and porous breakwaters, Coastal Engineering, 85, 12-29, ISSN 0378-3839, doi:10.1016/j.coastaleng.2013.12.003.

[56] Yakhot, V., Orszag, S.A., Thangam, S., Gatski, T.B., Speziale, C.G., 1992. Development of turbulence models for shear flows by a double expansion technique, Physics of Fluids A, 4(7), 1510-1520.

[57] Yip T.L., Chwang A.T. (2000). Perforated wall breakwater with internal horizontal plate. J. Eng. Mech. 126(5): 533–538. https://doi.org/10.1061/(ASCE)0733-9399(2000)126:5(533).